Biodistribution and Ultrastructural Localization of Single-Walled Carbon Nanohorns Determined *In Vivo* with Embedded Gd_2O_3 Labels

Jin Miyawaki,[†,#,⊥] Sachiko Matsumura,[†,‡,⊥] Ryota Yuge,[§] Tatsuya Murakami,[∥,▽] Shigeo Sato,[‡] Akihiro Tomida,[‡] Takashi Tsuruo,[‡] Toshinari Ichihashi,[§] Takako Fujinami,[¶] Hiroshi Irie,[⊥] Kunihiro Tsuchida,[∥] Sumio Iijima,[†,‡,¶] Kiyotaka Shiba,[‡,*] and Masako Yudasaka[†,§,¶,*]

[†]Japan Science and Technology Agency, Sanbancho Bldg., 5, Sanbancho Chiyoda-ku, Tokyo 102-0075, Japan, [‡]Japanese Foundation for Cancer Research, 3-10-6 Ariake, Koto-ku, Tokyo 135-8550, Japan, [§]NEC, 34 Miyukigaoka, Tsukuba 305-8501, Japan, [∥]Fujita Health University, Toyoake, Aichi 470-1192, Japan, [⊥]Teikyo University School of Medicine, 2-11-1 Kaga, Itabashi-ku, Tokyo 173-8605, Japan, and [¶]National Institute of Advanced Industrial Science and Technology, Central 5, 1-1-1 Higashi, Tsukuba 305-8565, Japan. [⊥]These authors contributed equally to this research. [#]Current address: Institute for Materials Chemistry and Engineering, Kyushu University, 6-1 Kasugakoen, Kasuga, Fukuoka 816-8580, Japan. [▽]Current address: Institute for Integrated Cell-Material Sciences (iCeMS), Kyoto University, Sakyo-ku, Kyoto 606-8304, Japan.

ABSTRACT Single-walled carbon nanohorns (SWNHs) are single-graphene tubules that have shown high potential for drug delivery systems. In drug delivery, it is essential to quantitatively determine biodistribution and ultrastructural localization. However, to date, these determinations have not been successfully achieved. In this report, we describe for the first time a method that can achieve these determinations. We embedded Gd_2O_3 nanoparticles within SWNH aggregates (Gd_2O_3@SWNHag) to facilitate detection and quantification. Gd_2O_3@SWNHag was intravenously injected into mice, and the quantities of Gd in the internal organs were measured by inductively coupled plasma atomic emission spectroscopy: 70−80% of the total injected material accumulated in liver. The high electron scattering ability of Gd allows detection with energy dispersive X-ray spectroscopy and facilitates the ultrastructural localization of individual Gd_2O_3@SWNHag with transmission electron microscopy. In the liver, we found that the Gd_2O_3@SWNHag was localized in Kupffer cells but were not observed in hepatocytes. In the Kupffer cells, most of the Gd_2O_3@SWNHag was detected inside phagosomes, but some were in another cytoplasmic compartment that was most likely the phagolysosome.

KEYWORDS: carbon nanohorn · ultrastructural observation · biodistribution · Gd_2O_3 · *in vivo* · carbon nanotube

A single-walled carbon nanohorn (SWNH) is a single-graphene tubule with a non-uniform diameter of 2−5 nm and a length of 40−50 nm. About 2000 SWNHs assemble to form a spherical aggregate with a diameter of about 100 nm (SWNHag).[1] Oxidation of SWNHs can open holes[2−4] that allow passage of various materials, including drugs, which can then be stored inside.[5−19] The local application of drug-incorporated SWNHs proved to be a highly effective therapy for tumors that had been subcutaneously transplanted in mice.[16−18] No acute toxicity of SWNHs has been observed in animal testings.[20,21] These results suggest that SWNHs exhibit high potential as drug delivery systems and may be useful for other biological applications. To enhance their potential therapeutic efficacies, SWNHs should be chemically functionalized and aggregate size should be optimized based on the biodistribution of SWNHs *in vivo*. In histological studies, SWNHs intravenously injected into mice were detected as black pigmentation in the lungs, liver, and spleen by optical microscopy, suggesting uptakes of SWNHs by tissue macrophages.[21] However, more precise ultrastructural localization and quantification are necessary to clearly identify the sites of uptake.

SWNHs do not have any intrinsic properties that are useful for detection; thus, they are difficult to quantify based on intrinsic properties. Multiwalled carbon nanotubes (MWNTs) and single-walled carbon nanotubes (SWNTs) with large diameters (>2 nm) also face the same problem. In contrast, SWNTs with narrow diameters[22,23] have intrinsic fluorescence[24,25] or Raman scattering of light emitted by photoexcitation,[26,27] allowing examinations of their *in vivo* biodistribution. It is possible to determine the biodistribution of SWNHs by chemically attaching label molecules, like

*Address correspondence to kshiba@jfcr.co.jp, m-yudasaka@aist.go.jp.

Received for review February 20, 2009 and accepted May 18, 2009.

Published online May 29, 2009.
10.1021/nn9004846 CCC: $40.75

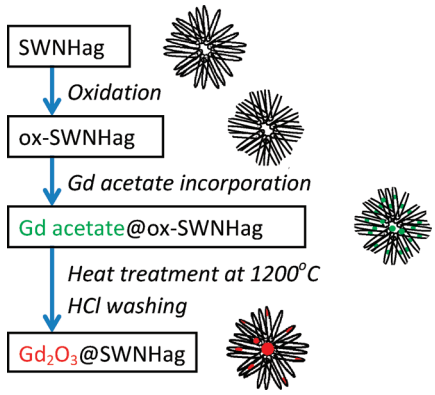

Figure 1. Process of Gd_2O_3@SWNHag preparation.

radioisotopes.[28,29] However, the attached molecules run the risk of detaching from the SWNHs while moving through the body, which gives rise to uncertainties in the measured values. In this report, we show that Gd_2O_3 nanoparticles embedded inside the SWNH aggregates[30] are excellent labels for SWNHs. Because they are embedded inside the SWNHag, Gd_2O_3 labels are unlikely to become detached from the SWNHag during movement through the body. We were able to determine SWNH biodistributions by measuring the quantity of Gd in the excised internal organs with inductively coupled plasma atomic emission spectroscopy (ICP-AES).

The embedded Gd_2O_3 in SWNHag also facilitated ultrastructural localization of SWNHag by transmission electron microscopy (TEM). The high electron scattering ability of Gd provided high contrast for clear detection by TEM and, because Gd is not found naturally in the body, it could be clearly identified with energy dispersive X-ray spectroscopy (EDX). The TEM coupled with elemental analysis by EDX or electron energy loss spectroscopy (EELS) is a conventional technique for localizing fine particles in various materials, including living tissues.[31−36]

Previous reports have been able to detect SWNTs[35] and MWNTs[37] in cells and tissues by TEM. The multiple graphene walls of MWNTs or bundles of SWNTs provided a high carbon density, and their long cylindrical structures were easily discriminated from tissue structures. Therefore, metal labels may not be in high demand for testing these molecules. However, it may be necessary to have concrete evidence to confirm that the cylindrical objects are actually graphene tubules. A study has used EELS to identify the π electrons in graphenes;[35] however, some ambiguities still remain because many materials have π electrons. For a more accurate identification of carbon tubules, these morphological observations and microscopic carbon energy analyses can be complemented with Gd labels or labels of other metals or compounds that are not found in the body and can be confined inside carbon nanotubes.

RESULTS AND DISCUSSION

Characterization of Gd_2O_3@SWNHag. A schematic of the Gd_2O_3-embedded SWNHag (Gd_2O_3@SWNHag) preparation is shown in Figure 1. The heat treatment at 1200 °C converted Gd acetate to Gd_2O_3 and closed the holes in the SWNHag, thus the Gd_2O_3 was embedded inside the SWNHag to form Gd_2O_3@SWNHag. Gd_2O_3@SWNHag enabled additional superior perfor-

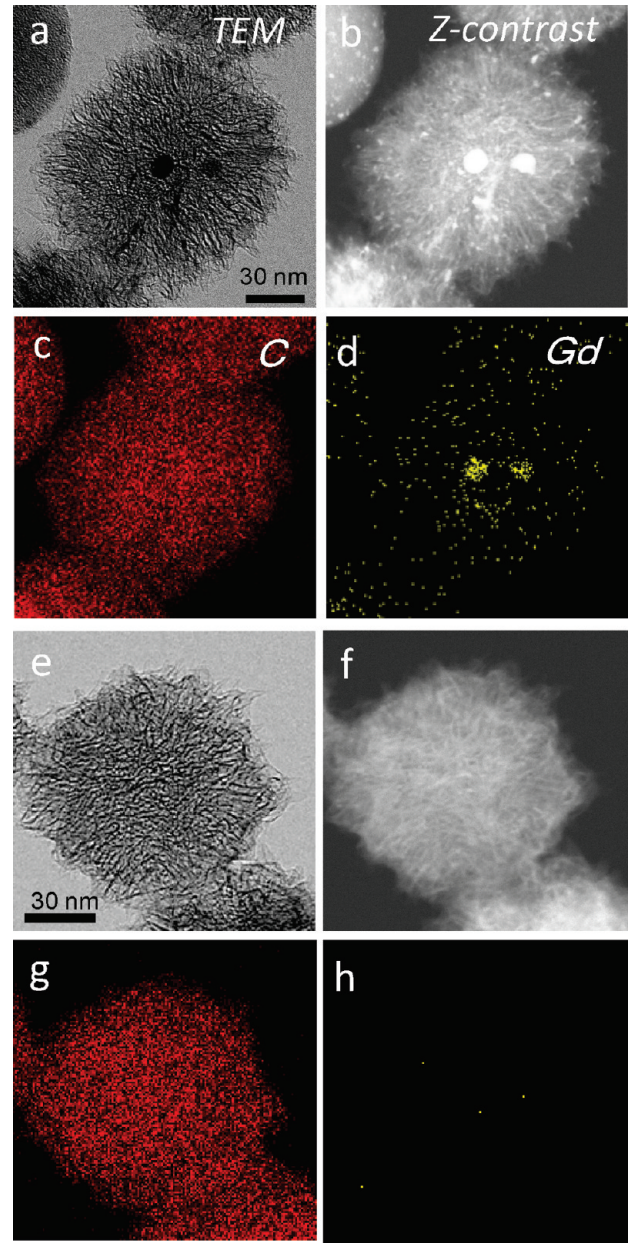

Figure 2. Microscopic structure of the Gd_2O_3@SWNHag powder: (a) TEM and (b) *Z*-contrast (ZC) images; (c) carbon and (d) Gd maps measured in the same area shown in (a) and (b); (e−h) similar images of SWNHag without Gd_2O_3 embeddings.

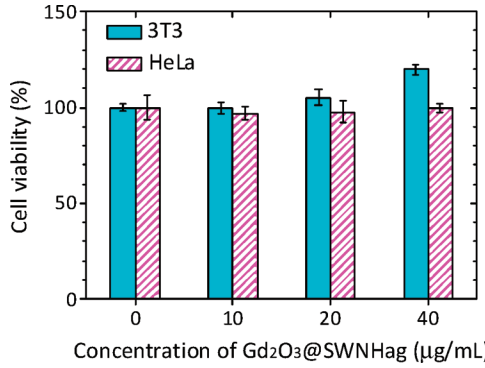

Figure 3. Cytotoxicity assessments of Gd_2O_3@SWNHag; 3T3 (pale blue) and HeLa (pink) cells were cultured with Gd_2O_3@SWNHag at different concentrations for 48 h. Cell viability was estimated with the WST-1 assay in triplicate. Error bars indicate mean square standard deviations.

mance for the *in vivo* study because it minimized the risk of Gd_2O_3 detachment from SWNHag.

The structure of Gd_2O_3@SWNHag has been previously shown by scanning transmission electron microscopy (STEM), electron diffraction analyses, and EELS measurements.[30] Many SWNHag had one or two large Gd_2O_3 nanoparticles (10−30 nm) near the center of the aggregate and small-sized nanoparticles (1−2 nm) scattered all over the aggregate. We found similar Gd_2O_3 distributions within our Gd_2O_3@SWNHag in STEM images (Figure 2a) and *Z*-contrast (ZC) images (Figure 2b); the Gd_2O_3 nanoparticles appeared as dark spots in the former and bright spots in the latter. We further confirmed the existence of Gd and carbon (C) elements with EDX. We found that the carbon was distributed all over the SWNHag (Figure 2c), and the large Gd_2O_3 particles were localized near the center of the SWNHag and small particles all over the aggregate (Figure 2d). Indeed, these Gd_2O_3 associated structural features were not found in pristine SWNHag (Figure 2e−h).

The cytotoxicity of Gd_2O_3@SWNHag was examined in the mouse fibroblast cell line, NIH 3T3, and the human cervical carcinoma cell line, HeLa. When these cells were incubated with Gd_2O_3@SWNHag dispersed in culture medium, no cytotoxicity was observed: the cell viability did not decrease with increasing Gd_2O_3@SWNHag quantities, as evaluated with the WST-1 assay (Figure 3).

Ultrastructural Localization of Gd_2O_3@SWNHag in Liver of Mouse. We injected *ca.* 0.2 mL of a glucose dispersion of Gd_2O_3@SWNHag (1 mg of Gd_2O_3@SWNHag in 1 mL of aqueous 5% glucose solution) into mice through the tail vein (dose: 10 mg of Gd_2O_3@SWNHag per 1 kg of body weight). Mice were sacrificed 14 days after the intravenous injection of Gd_2O_3@SWNHag. The livers were removed, and sections were dissected out for the optical microscopy observations. The images (Figure 4) showed black, micrometer-sized objects located in the hepatic sinusoids. We inferred that the black objects were agglomerates of Gd_2O_3@SWNHag that had been taken up by the Kupffer cells. This was confirmed in further studies with STEM and EDX (below).

Some excised tissues of liver were studied with STEM and EDX. We found that there were many globular objects in a phagosome, a vesicle with a homogeneous density that was surrounded by a limiting membrane (Figure 5a,b), located in a Kupffer cell in the hepatic sinusoidal spaces. The magnified images and EDX analysis of these globular objects (Figure 5c,d) showed the structures similar to those in Figure 2a−d, confirming that they were indeed the Gd_2O_3@SWNHag.

When the sizes of the Gd_2O_3 particles were small and their bright spots were not clearly discernible in the ZC images, the presence of Gd was confirmed by

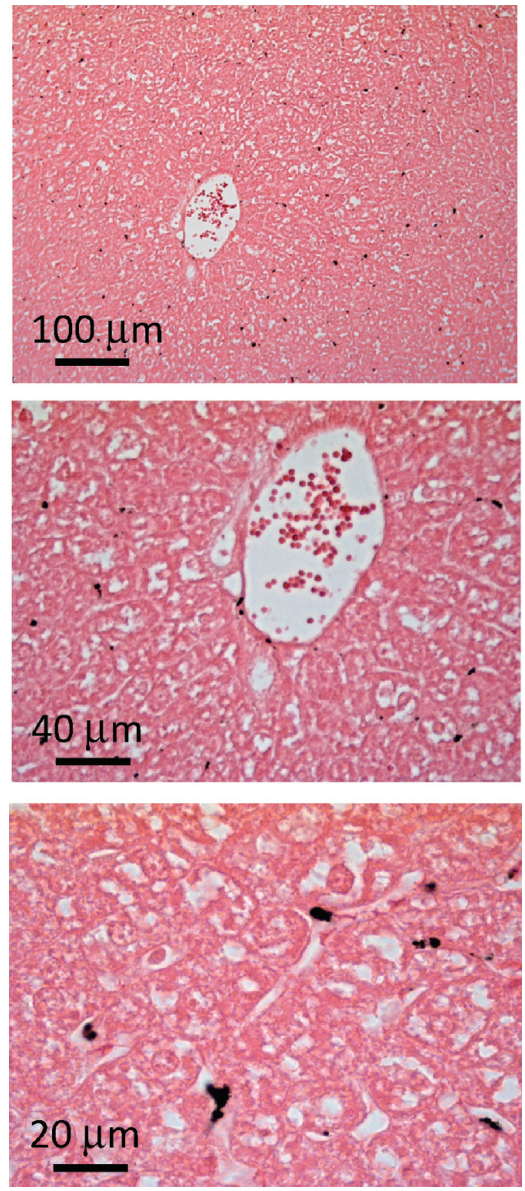

Figure 4. Optical microscopy images of mouse liver tissue. The liver was removed 14 days after Gd_2O_3@SWNHag administration into the tail vein (dose: 10 mg/kg body weight). Black particles are assumed to be Gd_2O_3@SWNHag.

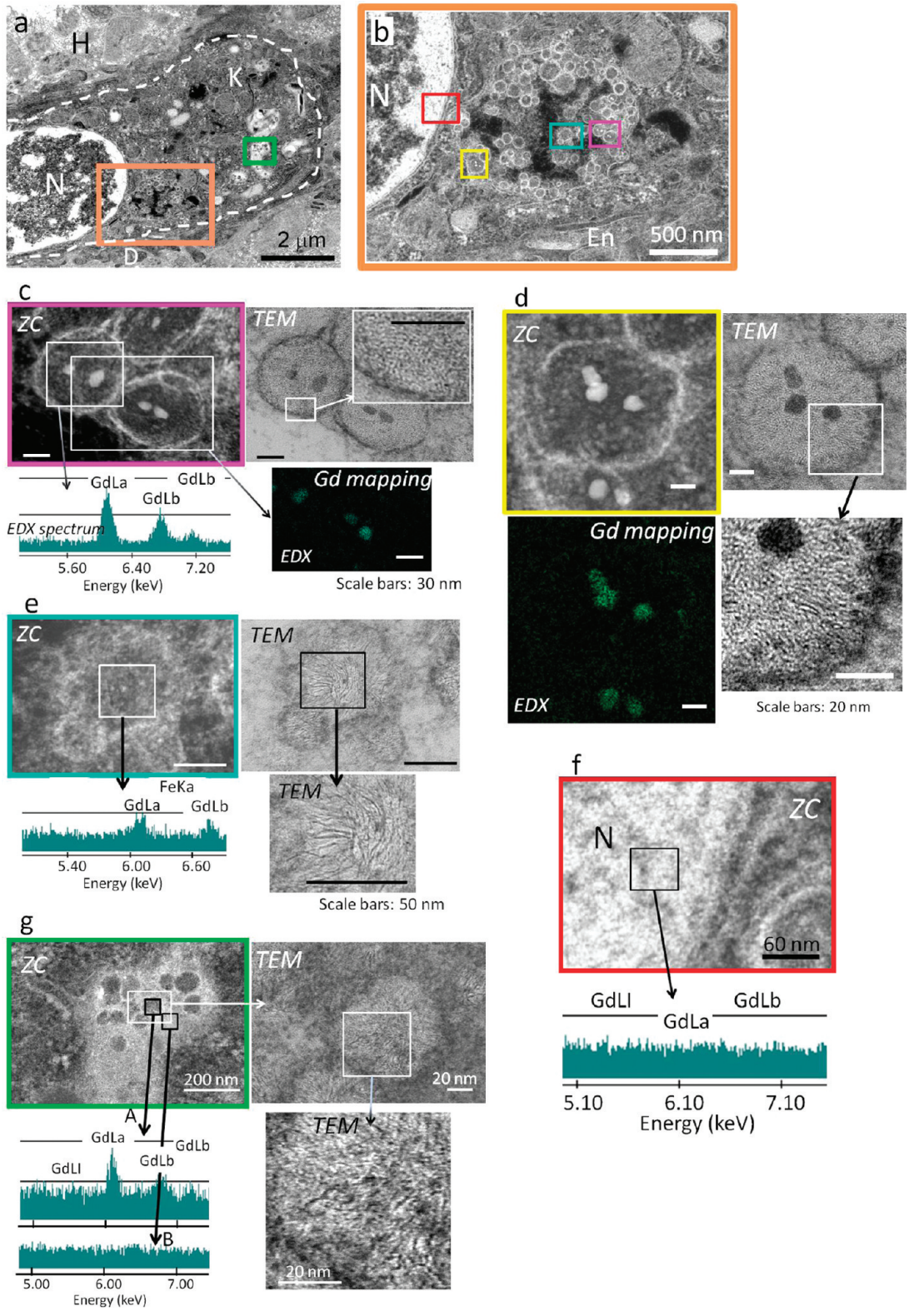

Figure 5. Ultrastructural localization of Gd_2O_3@SWNHag in mouse liver. (a) ZC image of mouse liver tissue. Kupffer cell (K) in a sinusoid is indicated with a white broken line. (b) Magnified image of the orange-framed area in (a). (c−g) ZC images, TEM images, EDX spectra, and Gd mapping of colored frames in (b) and (a). Gd_2O_3@SWNHag was intravenously injected into a mouse at a dose of 10 mg per kg body weight. The mouse was sacrificed after 14 days (H, hepatocytes; N, nucleus; D, perisinusoidal space of Disse; En, endothelial cell; K, Kupffer cell).

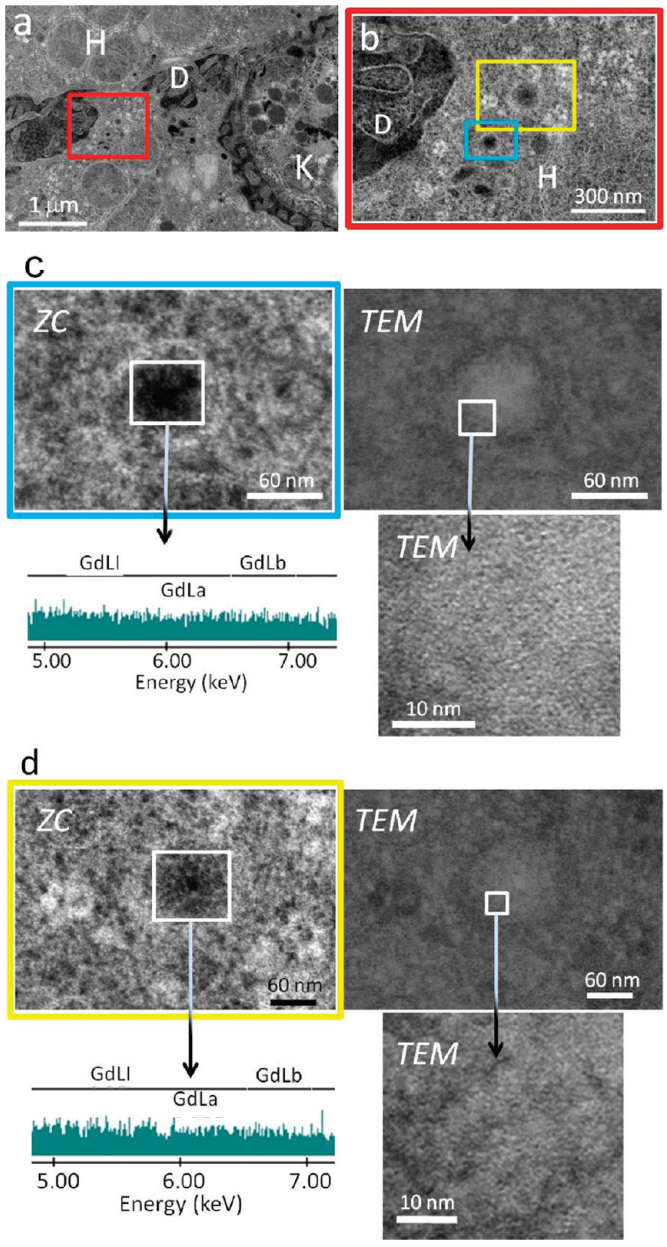

Figure 6. STEM observations of unidentified globular objects in mouse liver. (a) ZC image of mouse liver tissue. (b) ZC image of the red-framed area in (a). (c,d) ZC images, TEM images, and EDX spectra of the blue- and yellow-framed areas in (b). Gd_2O_3@SWNHag was intravenously injected into a mouse at a dose of 10 mg per kg body weight. The mouse was sacrificed after 14 days (H, hepatocytes; D, perisinusoidal space of Disse; K, Kupffer cell).

EDX spectrum measurements and the SWNHag structure was confirmed by TEM (Figure 5e).

The ZC images showed that Gd_2O_3@SWNHag was sometimes found in the cytoplasm, which appeared very bright, as shown in the orange-framed zone of Figure 5a and in the magnified images in Figure 5g. At present, we cannot be sure that this is the cytoplasm; however, we suspect that it may be a phagolysosome.

The inner edges of the Kupffer cell nucleus (Figure 5b, red-frame area) and the interior of phagolysosome-like cytoplasm (Figure 5a, orange-frame area) appeared bright in ZC images; therefore, it might be suspected that the Gd_2O_3 escaped out of the SWNHag and accumulated in these bright locations. However, the EDX analyses of these areas showed no inclusion of Gd (Figure 5f and Figure 5g,B) (see also Supporting Information, Figure 2e in SI.1).

Unidentified globular objects that were similar in size to SWNHag were sometimes found in liver tissues. They were examined with TEM, STEM, and EDX; however, the EDX did not detect any Gd, and high-resolution images showed no characteristic structures of SWNHag (Figure 6).

Several ultrastructural images of other liver regions are shown in the Supporting Information SI.1. We did not find any particles located outside of the Kupffer cells in our STEM observations.

We found that the ultrastructural localization of SWNHag was unambiguous among complex tissue structures with the Gd_2O_3 nanoparticle labels because the Gd_2O_3 are clearly localized by ZC observation and EDX measurements. We suggest that the ultrastructural localization of SWNHag previously presented by Lacotte *et al.*[38] could have been investigated more confidently with the use of Gd_2O_3 labels.

Distribution of Gd_2O_3@SWNHag in Mouse Body. The Gd_2O_3@SWNHag was quantified in the liver and other organs. The quantities of Gd_2O_3@SWNHag were estimated from the Gd quantities measured by ICP-AES as shown in Figure 7. The largest quantity of Gd_2O_3@SWNHag was found in the liver, representing 70−80% of the total injected quantity. The next largest quantity was found in the spleen, representing about 12% of the injected quantity. About 1−2% was found in the stomach/intestine or the lungs, and none was detected in the brain, heart, kidneys, or blood. These quantities did not change substantially throughout the test period, up to 7 days. This suggested that the Gd_2O_3@SWNHag was taken up by reticuloendothelial systems in the lungs, liver, and spleen within 30 min and remained stable for the 7 day period.

Although the Gd_2O_3@SWNHag quantities in the organs did not change substantially for 7 days (Figure 7), we did detect a slight decrease of Gd_2O_3@SWNHag in the lungs and a slight increase in the stomach/intestine (Figure 7b). The decrease of Gd_2O_3@SWNHag in the lungs suggested that the aggregates may have been exported from the lungs

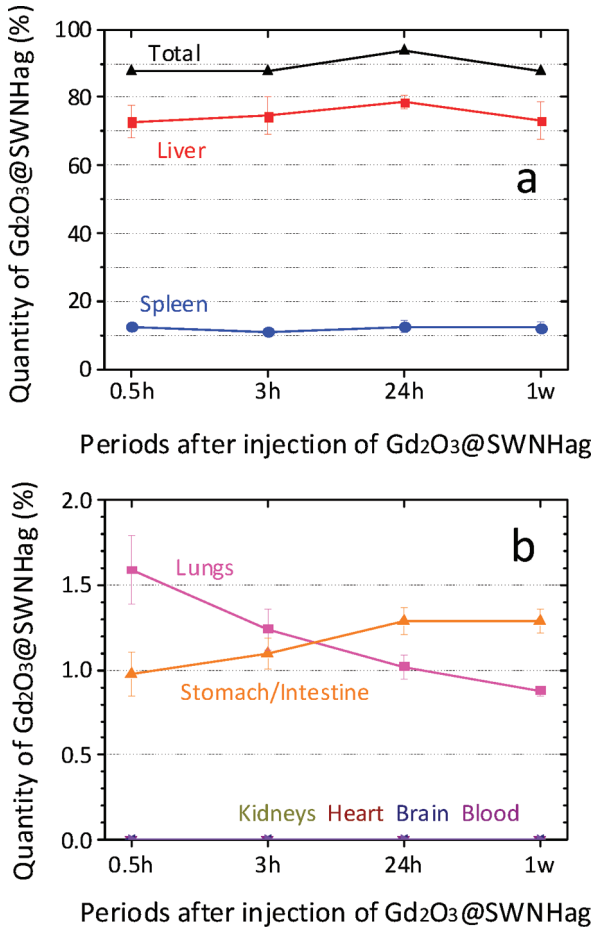

Figure 7. Biodistribution of Gd_2O_3@SWNHag in mice. Quantities of Gd_2O_3@SWNHag are expressed in weight % against the total injected quantity. (a) Quantities of Gd_2O_3@SWNHag in liver and spleen. (b) Quantities in brain, lungs, heart, kidneys, stomach/intestine, and blood. Error bars indicate mean square standard deviations. "Total" in (a) is the sum of quantities in the examined organs. Gd_2O_3@SWNHag was intravenously injected in mice ($n = 5$ for each period group) at a dose of 20 mg per kg body weight.

to other organs. Alternatively, those taken up by macrophages in the airways may have been excreted *via* respiration.[33]

The slight increase in the stomach/intestine might indicate that Gd_2O_3@SWNHag was excreted *via* a respiratory pathway, captured in sputum, and swallowed to reach the stomach and intestine. An alternate explanation could be that some of the Gd_2O_3@SWNHag in the liver was exported to the stomach/intestine through the gallbladder.

Our results indicate that Gd is a useful label, and Gd_2O_3-embedded SWNHag enabled the ultrastructural localization and quantification of SWNHag. Gd or Gd compounds have also been incorporated in a similar graphene material, SWNT.[39,40] We believe that the Gd and Gd compounds will be similarly useful in ultrastructural observations and biodistribution determinations of SWNTs. Clearly, other metals that are not naturally found in living bodies and that have high electron scattering properties may be comparable to Gd as labels, given that they can be properly enclosed inside carbon nanotubules.

CONCLUSION

The SWNH aggregates were labeled with embedded Gd_2O_3 nanoparticles. The Gd quantities in the internal organs of mice were measured with inductively coupled plasma atomic emission spectroscopy to make quantitative determinations of SWNH aggregate biodistributions. The results showed that, after an intravenous injection into the mouse tail vein, 70−80% of the total quantity of Gd_2O_3@SWNHag accumulated in the liver and about 10% in the spleen. Due to the high electron scattering property of Gd, the Gd_2O_3 nanoparticles were useful for the ultrastructural localization of SWNH aggregates. Scanning transmission electron microscopy and energy dispersive X-ray spectroscopy revealed that Gd_2O_3@SWNHag existed primarily in the phagosomes and sometimes in phagolysosome-like vacuoles of Kupffer cells in mice.

MATERIALS AND METHODS

Gd_2O_3 Confinements in SWNH Aggregates. SWNHag was prepared by CO_2 laser ablation of graphite without using metal catalysts.[1] The purity was about 90%, and 10% included micrometer-sized graphitic particles.[2,3] The holes were opened in the walls of SWNHag (ox-SWNHag) by oxidation with oxygen gas (760 Torr, 200 mL/min) at 500 °C for 10 min.[3]

The preparation of Gd-oxide-embedded SWNHag (Figure 1) was described elsewhere.[10] Briefly, Gd acetate (50 mg) and ox-SWNHag (50 mg) were dispersed in ethanol (20 mL), stirred at room temperature for 12 h, followed by filtration and washing with ethanol. The ox-SWNHag and incorporated Gd acetate was dried and heat treated at 1200 °C in Ar for 3 h. The heat treatment at 1200 °C in Ar removed the oxygenated groups and closed the holes of ox-SWNHag. This caused the Gd_2O_3 to remain embedded in SWNHag. The product weighed *ca.* 60 mg. We prepared the specimen until the heat treatment step once more to secure enough amount for all characterization and *in vitro*/*in vivo* studies. To remove the excess Gd_2O_3 on the outer surfaces, Gd_2O_3@SWNHag (110 mg) was sonicated for about 30 min in 35−37% aqueous HCl solution (500 mL) followed by washing with water (500 mL). This process was repeated three times. The final product was designated Gd_2O_3@SWNHag.

The quantities of Gd_2O_3 trapped in the Gd_2O_3@SWNHag were estimated to be about 7% from thermogravimetric analysis (TGA) (Supporting Information, SI.2) and 7.1% measured by ICP-AES (ULTIMA 2, Horiba Co.). For the ICP-AES measurements, the Gd_2O_3@SWNHag was combusted at 900 °C in air for 4 h, and the resulting ash was dissolved in 5 mL of an aqueous solution of HCl (35−37%, atomic absorption grade, Kanto Chemical Co., Inc.). Then, 4.5 mL of the solution was batched off and diluted with 4.5 mL of ultrapure water. The Gd emission intensity in ICP-AES was calibrated at 310.050 nm from a calibration curve constructed using $Gd(NO_3)_3$ solutions with concentrations of 0.01−5 ppm prepared by diluting standard $Gd(NO_3)_3$ nitrate solutions

(1 mg of Gd in 1 mL of HNO_3 solution, Gd atomic absorption standard solution, Sigma-Aldrich) with ultrapure water.

The structure of Gd_2O_3@SWNHag was confirmed with STEM (HD2300, Hitachi) at a 120 keV acceleration voltage and about 64 μA current. Mapping the elements of Gd and C was performed with EDX (Genesis 4000, EDAX) equipped on the STEM.

Cytotoxicity Assay. The cytotoxicity of Gd_2O_3@SWNHag was evaluated with a WST-1 (4-[3-(4-iodophenyl)-2-(4-nitrophenyl)-2*H*-5-tetrazolio]-1,3-benzene disulfonate) assay (Roche Diagnostics) for a mouse fibroblast cell line, NIH 3T3, and a human cervical carcinoma cell line, HeLa. This colorimetric assay quantified cell proliferation and cell viability based on the reduction of WST-1 into formazan by the mitochondrial succinate-tetrazolium-reductase system in living cells. The cells were seeded in complete medium; for NIH 3T3 cells, the medium comprised D-MEM (11995, GIBCO), 10% bovine serum (16170-078, GIBCO), 100 U/mL penicillin, and 100 μg/mL streptomycin (15070-063, GIBCO). For HeLa cells, the medium comprised MEM (M4655, SIGMA), 10% bovine serum (16170-078, GIBCO), 100 U/mL penicillin, and 100 μg/mL streptomycin (15070-063, GIBCO). Aliquots (100 μL) of cells suspended at a concentration of 1×10^5 cell/mL for NIH 3T3 and 4×10^4 cell/mL for HeLa were placed in each well of 96-well microplates and were incubated at 37 °C in humidified air with 5% CO_2 for 24 h. After removal of the culture medium from the 96-well microplates, 100 μL of the Gd_2O_3@SWNHag (0, 10, 20, and 40 mg/mL) dispersed in medium was added to each well, followed by incubation at 37 °C in 5% CO_2 for 48 h. After the 48 h incubation, 10 μL of the WST-1 was added to the wells. After incubation for 3 h (3T3) or 1 h (HeLa), the cell viabilities were monitored by measuring light absorbance at 450 nm with a microplate reader (Model 680 microplate reader, Bio-Rad). The base absorbance was taken at 620 nm.

Histological and Ultrastructural Analyses of Liver Tissues. Female, 6 week old mice (BALB/cAnNCrlCrlj) were purchased from Charles River Laboratories, Japan, and housed for another 2 weeks at the Cancer Research Institute or Fujita Health University in accordance with the regulations of the committees on the Use and Care of Animals. Animals were fed *ad libitum* with γ-irradiated rodent diet CE2 (CLEA Japan Inc.).

We injected *ca.* 0.2 mL of a glucose dispersion of Gd_2O_3@SWNHag (1 mg of Gd_2O_3@SWNHag in 1 mL of aqueous 5% glucose solution) into 8 week old mice through the tail vein (dose: 10 mg of Gd_2O_3@SWNHag per 1 kg of body weight, number of mice $n = 1$). The Gd_2O_3@SWNHag was highly dispersed in 5% glucose solution (Supporting Information, SI.3). Mice were sacrificed 14 days after the intravenous injection of Gd_2O_3@SWNHag. The livers were removed, fixed in 10% neutral buffered formalin for >24 h, embedded in paraffin, and cut into 4 μm sections. Eosin-stained sections were analyzed by optical microscopy.

Some excised tissues of liver were fixed by immersion in 2% glutaraldehyde in 0.1 M phosphate buffer overnight at 4 °C then in osmium tetraoxide solution (1, 70, and 100% each for 30 min), propylene oxide (1 h, twice), and Epon embedding solution (3 days, 60 °C). The Epon-embedded blocks were sliced (LKB U5 Ultramicrotome) at 80−100 nm thick followed by staining with uranyl acetate for 10 min and Reynolds lead for 3 min. The sections were analyzed by STEM, and the mapping of Gd and C elements was performed with EDX.

Distribution of Gd_2O_3@SWNHag in the Mouse Body. Another group of the same species of mice was similarly treated with a higher dose of Gd_2O_3@SWNHag (dose: 20 mg of Gd_2O_3@SWNHag per 1 kg of body weight). As a control, one group of mice was injected intravenously with *ca.* 0.2 mL of the 5% aqueous glucose solution. The mice were sacrificed at 0.5 h, 3 h, 24 h, or 1 week ($n = 5$ for each group) after the Gd_2O_3@SWNHag injection. We removed the brain, heart, lungs, liver, spleen, kidneys, and stomach/intestine. Before the dissection, about 1 mL of blood was collected and preserved with an anticoagulant of heparin. The specimens were dried at about 120 °C in air, followed by combustion at 900 °C in air for 4 h. The Gd quantity in the ash was measured with ICP-AES, as described above.

Acknowledgment. We thank Dr. Azami and Dr. Kasuya (NEC Co.) for the preparation of SWNHs, and Ms. Minamisawa (Japanese Foundation for Cancer Research) for preparing the tissue slices for histological observations.

Supporting Information Available: STEM *Z*-contrast (ZC) images with EDX and EELS measurements of a mouse liver, ICP-AES spectra of excrements of mice, TGA results of Gd_2O_3@SWNHag, and dynamic light scattering of Gd_2O_3@SWNHag in 5% glucose solution. This material is available free of charge *via* the Internet at http://pubs.acs.org.

REFERENCES AND NOTES

1. Iijima, S.; Yudasaka, M.; Yamada, R.; Bandow, S.; Suenaga, K.; Kokai, F.; Takahashi, K. Nano-Aggregates of Single-Walled Graphitic Carbon Nano-Horns. *Chem. Phys. Lett.* **1999**, *309*, 165–170.
2. Utsumi, S.; Miyawaki, J.; Tanaka, H.; Hattori, Y.; Ito, T.; Ichikuni, N.; Kanoh, H.; Yudasaka, M.; Iijima, S.; Kaneko, K. Opening Mechanism of Internal Nanoporosity of Single-Wall Carbon Nanohorn. *J. Phys. Chem. B* **2005**, *109*, 14319–14324.
3. Fan, J.; Yudasaka, M.; Miyawaki, J.; Ajima, K.; Murata, K.; Iijima, S. Control of Hole Opening in Single-Wall Carbon Nanotubes and Single-Wall Carbon Nanohorns Using Oxygen. *J. Phys. Chem. B* **2006**, *110*, 1587–1591.
4. Ajima, K.; Yudasaka, M.; Suenaga, K.; Kasuya, D.; Azami, T.; Iijima, S. Materials Storage Mechanism in Porous Nanocarbons. *Adv. Mater.* **2004**, *16*, 397–401.
5. Murata, K.; Hirahara, K.; Yudasaka, M.; Iijima, S.; Kasuya, D.; Kaneko, K. Nanowindow-Induced Molecular Sieving Effect in a Single-Wall Carbon Nanohorn. *J. Phys. Chem. B* **2002**, *106*, 12668–12669.
6. Yang, C. M.; Kim, Y. J.; Endo, M.; Kanoh, H.; Yudasaka, M.; Iijima, S.; Kaneko, K. Nanowindow-Regulated Specific Capacitance of Supercapacitor Electrodes of Single-Wall Carbon Nanohorns. *J. Am. Chem. Soc.* **2007**, *129*, 20–21.
7. Yudasaka, M.; Fan, J.; Miyawaki, J.; Iijima, S. Studies on the Adsorption of Organic Materials inside Thick Carbon Nanohotubes. *J. Phys. Chem. B* **2005**, *109*, 8909–8913.
8. Murata, K.; Kaneko, K.; Kanoh, H.; Kasuya, D.; Takahashi, K.; Kokai, F.; Yudasaka, M; Iijima, M. Adsorption Mechanism of Supercritical Hydrogen in Internal and Interstitial Nanospaces of Single-Wall Carbon Nanohorns Assembly. *J. Phys. Chem. B* **2002**, *106*, 11132–11138.
9. Bekyarova, E.; Murata, K.; Yudasaka, M.; Kasuya, D.; Iijima, S.; Tanaka, H.; Kanoh, H.; Knaneko, K. Single-Wall Nanostructured Carbon for Methane Storage. *J. Phys. Chem. B* **2003**, *107*, 4682–4684.
10. Bekyarova, E.; Hanzawa, Y.; Kaneko, K.; Albero, J. S.; Escribano, A. S.; Reinoso, F. R.; Kauysa, D.; Yudasaka, M.; Iijima, S. Cluster-Mediated Filling of Water Vapor in Intra-Tube and Interstitial Nanospaces of Single-Wall Carbon Nanohorns. *Chem. Phys. Lett.* **2002**, *366*, 463–468.
11. Yudasaka, M.; Ajima, K.; Suenaga, K.; Ichihashi, T.; Hashimoto, A.; Iijima, S. Nano-Extraction and Nano-Condensation for C_{60} Incorporation into Single-Wall Carbon Nanotubes in Liquid Phases. *Chem. Phys. Lett.* **2003**, *380*, 42–46.
12. Hashimoto, A.; Yorimitsu, H.; Ajima, K.; Suenaga, K.; Isobe, H.; Miyawaki, J.; Yudasaka, M.; Iijima, S.; Nakamura, E. Selective Deposition of a Gadolinium(III) Cluster in a Hole Opening of Single-Wall Carbon Nanohorn. *Proc. Natl. Acad. Sci. U.S.A.* **2004**, *101*, 8527–8530.
13. Yuge, R.; Ichihashi, T.; Shimakawa, Y.; Kubo, Y.; Yudasaka, M.; Iijima, S. Preferential Deposition of Pt Nanoparticles inside Single-Wall Carbon Nanohorns. *Adv. Mater.* **2004**, *16*, 1420–1423.
14. Murakami, T.; Ajima, K.; Miyawaki, J.; Yudasaka, M.; Iijima, S.; Shiba, K. Drug-Loaded Carbon Nanohorns: Adsorption and Release of Dexamethasone *In Vitro*. *Mol. Pharm.* **2004**, *1*, 399–405.
15. Ajima, K.; Yudasaka, M.; Murakami, T.; Maigne, A.; Shiba, K.; Iijima, S. Carbon Nanohorns as Anticancer Drug Carriers. *Mol. Pharm.* **2005**, *2*, 475–480.

16. Murakami, T.; Sawada, H.; Tamura, G.; Yudasaka, M.; Iijima, S.; Tsuchida, K. Water-Dispersed Single-Wall Carbon Nanohorns as Drug Carriers for Local Cancer Chemotherapy. *Nanomedicine* **2008**, *3*, 453–463.
17. Ajima, K.; Murakami, T.; Mizoguchi, Y.; Tsuchida, K.; Ichihashi, T.; Iijima, S.; Yudasaka, M. Enhancement of *In Vivo* Anticancer Effects of Cisplatin by Incorporation inside Single-Wall Carbon Nanohorns. *ACS Nano* **2008**, *2*, 2057–2064.
18. Zhang, M.; Murakami, T.; Ajima, K.; Tsuchida, K.; Sandanayaka, A. S. D.; Ito, O.; Iijima, S.; Yudasaka, M. Fabrication of ZnPc/Protein Nanohorns for Double Photodynamic and Hyperthermic Cancer Phototherapy. *Proc. Natl. Acad. Sci. U.S.A.* **2008**, *105*, 14773–14778.
19. Xu, J.; Yudasaka, M.; Kouraba, S.; Sekido, M.; Yamamoto, Y.; Iijima, S. Single Wall Carbon Nanohrn as a Drug Carrier for Controlled Release. *Chem. Phys. Lett.* **2008**, *461*, 189–192.
20. Miyawaki, J.; Yudasaka, M.; Azami, T.; Kubo, Y.; Iijima, S. Toxicity of Single-Walled Carbon Nanohorns. *ACS Nano* **2008**, *2*, 213–226.
21. Miyawaki, J.; Yudasaka, M.; Zhang, M.; Iijima, S. Intravenous Toxicity of Single-Walled Carbon Nanohorns. *The 34th Fullerene-Nanotube Symposium*, 2007.
22. Iijima, S. Helical Micro Tubules of Graphitic Carbon. *Nature* **1991**, *354*, 56–58.
23. Iijima, S; Ichihashi, T. Single-Shell Carbon Nanotubes of 1-nm Diameter. *Nature* **1993**, *363*, 603–605.
24. Cherukuri, P.; Gannon, C, J,; Leeuw, T. K.; Schmidt, H. K.; Smalley, R. E.; Curley, S. A.; Weisman, R. B. Mammalian Pharmacokinetics of Carbon Nanotubes Using Intrinsic Near-Infrared Fluorescence. *Proc. Natl. Acad. Sci. U.S.A.* **2006**, *103*, 18882–18886.
25. Leeuw, T. K.; Reith, R. M.; Simonette, R. A.; Harden, M. E.; Cherukuri, P.; Ttsyboulski, T. A.; Beckingham, K. E.; Weiseman, R. B. Single-Walled Carbon Nanotubes in the Intact Organism: Near-IR Imaging and Biocompatibility. *Nano Lett.* **2007**, *7*, 2650–2654.
26. Liu, Z.; Davis, C.; Cai, W.; Chen, L.; Dai, H. Circulation and Long-Term Fate of Functionalized, Biocompatible Single-Walled Carbon Nanotubes in Mice Probed by Raman Spectroscopy. *Proc. Natl. Acad. Sci. U.S.A.* **2008**, *105*, 1410–1415.
27. Liu, Z.; Chen, K.; Davis, C.; Sherlock, S.; Cao, Q. Z.; Chen, X. Y.; Dai, H. J. Drug Delivery with Carbon Nanotubes for *In Vivo* Cancer Treatment. *Cancer Res.* **2008**, *68*, 6652–6660.
28. Singh, R.; Pantarotto, D.; Lacerda, L.; Pastorin, G.; Klumpp, C.; Prato, M.; Bianco, A.; Kostarelos, K. Tissue Biodistribution and Blood Clearance Rates of Intravenously Administered Carbon Nanotube Radiotracers. *Proc. Natl. Acad. Sci. U.S.A.* **2006**, *103*, 3357–3362.
29. Liu, Z.; Cai, W.; He, L.; Nakayama, N.; Chen, K.; Sun, X.; Chen, X.; Dai, H. *In Vivo* Biodistribution and Highly Efficient Tumour Targeting of Carbon Nanotubes in Mice. *Nat. Nanotechnol.* **2006**, *2*, 47–52.
30. Yuge, R.; Ichihashi, R.; Miyawaki, J.; Yoshitake, T.; Iijima, S.; Yudasaka, M. Hidden Caves in an Aggregate of Single-Wall Carbon Nanohorns Found by Using Gd_2O_3 Probes. *J. Phys. Chem. C* **2009**, *113*, 2741–2744.
31. Irie, H.; Mori, W. Long Term Effects of Thorium Dioxide (Thorotrast) Administration on Heman Liver. *Acta Pathol. Jpn.* **1984**, *34*, 221–228.
32. Yamamoto, M.; Kato, K.; Ikada, Y. Ultrastructure of the Interface between Cultured Osteoblasts and Surface-Modified Polymer Substrates. *J. Biomed. Mater. Res.* **1997**, *37*, 29–36.
33. Irie, H. Delayed Effect of Thorotrast Deposition in Humans: Carcino-Genesis and Suppression of the Reticuloentdothelial System. *Biosci. Microflora* **2000**, *19*, 107–116.
34. Leize, E. M.; Hemmerle, J; Leize, M. Characterization, at the Bone Crystal Level, of the Titanium-Coating/Bone Interfacial Zone. *Clin. Oral Impl. Res.* **2000**, *11*, 279–288.
35. Porter, A. E.; Gass, M.; Muller, K.; Skepper, J. N.; Midgley, P. A.; Welland, M. Direct Imaging of Single-Walled Carbon Nanotubes in Cells. *Nat. Nanotechnol.* **2007**, *2*, 713–717.
36. Thakaral, C.; Abraham, J. L. Automated Scanning Electron Microscopy and X-ray Microanalysis for *In-Situ* Quantification of Gadolinium Deposits in Skin. *J. Electron Microsc.* **2007**, *56*, 181–187.
37. Lacerda, L.; Herrero, M. A.; Venner, K.; Biamco, A.; Prato, M.; Kostarelos, K. Carbon-Nanotube Shape and Individualization Critical for Renal Excretion. *Small* **2008**, *4*, 1130–1132.
38. Lacotte, S.; Garcia, A.; Decossas, M.; Al-Jamal, W.; Li, S.; Kostarelos, K.; Muller, S.; Prato, M.; Dumortier, H.; Bianco, A. Interfacing Functionalized Carbon Nanohorns with Primary Phagocytic Cells. *Adv. Mater.* **2008**, *20*, 2421–2426.
39. Suenaga, K.; Tence, T.; Mory, C.; Colliex, C.; Kato, H.; Okazaki, T.; Shinohara, H.; Hirahara, K.; Bandow, S.; Iijima, S. Element-Selective Single Atom Imaging. *Science* **2000**, *290*, 2280–2282.
40. Kitaura, R.; Imazu, N.; Kobayashi, K.; Shinohara, H. Fabrication of Metal Nanowires in Carbon Nanotubes *via* Versatile Nano-Template Reaction. *Nano Lett.* **2008**, *8*, 693–699.